Res Chem Intermed (2016) 42:4513–4530
DOI 10.1007/s11164-015-2293-x

Removal of mercury and fluoride from aqueous solutions by three-dimensional reduced-graphene oxide aerogel

Shibiao Wu[1,2] · Lingtao Kong[2] · Jinhuai Liu[1,2]

Received: 30 May 2015 / Accepted: 21 September 2015 / Published online: 12 October 2015

Abstract Three-dimensional reduced-graphene oxide (3-D RGO) hydrogel was synthesized by hydrothermal method from graphene oxide, de-ionized water, and oxalic acid dehydrate. The porous and low-density 3-D RGO aerogel was prepared after the RGO hydrogel was freeze-dried. The application of the 3-D RGO aerogel as an adsorbent for the removal of the inorganic ions, mercury(II) cation (Hg^{2+}), and fluoride anions (F^{-}), from aqueous solutions was investigated. The results revealed that the 3-D RGO aerogel showed excellent removal capabilities for Hg^{2+} and F^{-}. The adsorption data could be well described by the pseudo-second-order model, and the adsorption isotherms followed the Langmuir model better than the Freundlich model. The maximum adsorption capability of Hg^{2+} and F^{-} approached 185 and 31.3 mg g^{-1}, respectively, indicating that the 3-D RGO aerogel is a very suitable material for environmental pollution management.

Keywords Graphene · Aerogel · Adsorption · Mercury · Fluoride

Introduction

With fast development of industry, wastewater from various industries such as metal finishing, electroplating, plastics, and mining, containing several harmful ions of health and environmental concern such as mercury [1], cadmium, copper,

✉ Lingtao Kong
ltkong@iim.ac.cn

[1] College of Chemistry and Chemical Engineering, Anhui University, Hefei 230601, Anhui, People's Republic of China

[2] Nanomaterials and Environmental Detection Laboratory, Institute of Intelligent Machines, Chinese Academy of Sciences, Hefei 230031, Anhui, People's Republic of China

chromium, zinc, nickel [2], fluoride [3], arsenic [4], and other ions, have been discharged in environment with an increasing amount.

Mercury is a leading concern among the toxic heavy metals because of its volatility, persistence, bioaccumulation in the environment, and its neurological health impacts [5]. Though fluorine is a trace element necessary for human teeth and skeleton, a number of diseases, such as fluorosis of bone and cancer [6], are caused by ingestion of water contaminated with excess fluoride. Therefore, mercury and fluorine pollution has aroused global concern, and the removal of mercury and fluorine ions from water environment has become an urgent need to meet.

To alleviate the problem of water pollution by the harmful ions in the environment, various methods have been used to remove the ions from wastewater, such as electrocoagulation [7–9] and flocculation [10], adsorption [11], ion exchange [12], reverse osmosis [13], and electrodialysis [14].

Among the methods, the adsorption method is a promising technology. The major advantages of the adsorption technique are its low cost, simplicity of operation, low generation of residues, and recycling of the adsorbent [15]. Recently, many new adsorbents have been developed which show promise in treating waste water [16, 17]. Graphene, as one of novel carbon materials, is a versatile material with unique electronic, mechanical, optical, thermal, magnetic, and biocompatibility properties [18–30]. Because of high specific surface area, graphene is an excellent adsorbent for organic [15] and inorganic pollutants [31–34].

In this paper, three-dimensional self-assembled reduced-graphene oxide (3-D RGO) hydrogel [35] and aerogel [36] were prepared, and the adsorption abilities of the 3-D RGO aerogel for Hg^{2+} and F^{-} ions in water were also investigated.

Experimental

Materials

Graphite powder, 325 mesh, 99.8 % (metals basis) was purchased from Alfa Aesar. Sodium nitrate ($NaNO_3$), potassium permanganate ($KMnO_4$), concentrated sulfuric acid (98 % H_2SO_4), hydrogen peroxide (30 % H_2O_2), hydrochloric acid (HCl), nitric acid (HNO_3), sodium hydroxide (NaOH), oxalic acid dihydrate (OA), mercuric nitrate ($HgNO_3$), and sodium fluoride (NaF) were purchased from Shanghai Chemical Reagents Company, and were used directly without further purification. All the reagents were of analytical grade and used without further purification. Ultra-pure water (18.25 MΩ cm) was produced using a PSDK System (PSDK-C, Beijing, China).

Preparation of graphite oxide (GO)

GO was prepared by oxidation of natural graphite powder (325 mesh) according to a modified Hummers' method [37]. Briefly, graphite (1.0 g) was added to concentrated sulfuric acid (46 ml) under stirring at room temperature for 12 h. Then, sodium nitrate (1 g) was added, and the mixture was cooled to 0 °C. Under vigorous

agitation, potassium permanganate (6.0 g) was added slowly to keep the temperature of the suspension lower than 20 °C. Successively, the reaction system was transferred to a 35 °C water bath for about 1 h, forming a thick paste. Then, 80 ml of water was added, the reaction system was transferred to a 90 °C water bath for about 1 h. An additional 200 ml of water was added and followed by a slow addition of 6 ml of H_2O_2 (30 %), turning the color of the solution from brown to yellow. The mixture was filtered and washed with 1:10 HCl aqueous solution (250 ml) to remove metal ions followed by repeated washing with water and centrifugation to remove the acid until the pH value of supernatant became neutral. The resulting solid was dispersed in water by ultrasonication for 1.5 h to make a GO aqueous dispersion (15 mg ml^{-1}). The obtained brown dispersion was then subjected to 30 min of centrifugation at 4000 rpm to remove any aggregates. Finally, it was purified by dialysis for 1 week to remove the remaining salt impurities.

Synthesis of 3-D RGO hydrogel and aerogel

Fifty milligrams of OA was added into a 40-ml vial containing 20 ml 1.5 mg ml^{-1} GO aqueous solution with vigorous magnetic stirring for several minutes until completely dissolved. The homogeneous GO aqueous dispersion was sealed in a 60-ml Teflon-lined autoclave and maintained at 140 or 180 °C for 2 h. Then the autoclave was naturally cooled to room temperature and the as-prepared 3-D RGO hydrogel cylinder was purified by dialysis for 3 days to remove the remaining OA impurities. For aerogel preparation, the purified 3-D RGO hydrogel cylinder was freeze-dried to remove absorbed water and became 3-D RGO aerogel cylinder.

Characterization

The structure and overall crystallinity in the aerogel powder were characterized operated on an X-ray diffractometer (Y-2000, Dandong Radiative Instrument Group Co. Ltd. Liaoning, PRC) with Cu-K_α radiation. The powder morphology was investigated through scanning electron microscopy on a field-emission SEM (Sirion200, FEI Company, USA) operated at 5 kV voltage value. The rheology properties were also studied by a mechanical testing machine (Instron-3369, Instron Corporation, USA). The molecular structure of the products was detected with Fourier transform infrared (FT-IR) spectra (Nexus-870, Nicolet Company, USA). A Rex pH meter (PHB-4, Shanghai, China) was used for pH value detection.

Adsorption kinetics experiments

$HgNO_3$ and NaF powder were dissolved in ultra-pure water to prepare Hg^{2+} and F^- aqueous solution, respectively. Initial pH values of the Hg^{2+} or F^- solutions in the adsorption experiments were adjusted to 6.0, by adding HNO_3 or NaOH aqueous solution.

One hundred milliliters of Hg^{2+} or F^- aqueous solution mixed with an appropriate amount of sorbent (3-D RGO aerogel) was stirred by an electromagnetic

agitator with a speed of 800 round per minute in a sealed plastic flask at 25 °C. The mixtures of the sorbent and Hg^{2+} or F^- solution were separated by filtration for sampling at defined intervals.

The concentrations of Hg^{2+} and F^- ions were determined by inductively coupled plasma atomic emission spectrometry (ICPS-7000; Shimadzu Corp. Japan) and fluoride ions selective electrode (F001502; Van London-pHoenix Corp. USA), respectively.

Adsorption isotherms experiments

One hundred milliliters of Hg^{2+} or F^- aqueous solution mixed with 20 mg sorbent (3-D RGO aerogel) was shaken by an oscillator in a sealed plastic flask at 25 °C for 24 h. The pH condition was the same as the kinetic experiments. The initial and final concentrations of Hg^{2+} or F^- were detected as mentioned above.

Adsorption thermodynamics experiments

One hundred milliliters of Hg^{2+} or F^- aqueous solution mixed with 20 mg sorbent (3-D RGO aerogel) was shaken by an oscillator in a sealed plastic flask at 298, 308, and 318 K for 24 h. Other experiment conditions were the same as mentioned above.

Regeneration experiments

The first round of adsorption and desorption:

Adsorption: the initial dosages of adsorbent (3-D RGO aerogel) were 100 mg in 100 ml aqueous solution; 10 ppm Hg^{2+} or 5 ppm F^- aqueous solution mixed with sorbent (RGO aerogel) was shaken by an oscillator in a sealed plastic flask at 25 °C for 24 h. The pH condition was the same as above. The concentrations of Hg^{2+}or F^- were detected as mentioned above.
Desorption: the adsorbent was then filtered by suction filtration and cleaned with 500 ml of ultra-pure water; 100 ml 0.2 M HNO_3 (for Hg^{2+} desorption) or 0.2 M NaOH aqueous solution (for F^- desorption) mixed with the 3-D RGO aerogel filter cake was stirred by an electromagnetic agitator in a sealed plastic flask for adsorbent regeneration at 25 °C for 24 h. The adsorbent was filtered again by suction filtration and cleaned with enough ultra-pure water until the pH value of filtrate became neutral. The filter cake would be freeze-dried to remove absorbed water and used as the adsorbent in the second round of adsorption and desorption.

The second, third, fourth, and fifth round of adsorption and desorption were carried out like the first round.

Results and discussion

Process optimization for lower density of RGO aerogel

The reduction of GO by reducing agents, such as L-ascorbic acid, $NaHSO_3$, Na_2S and sodium ascorbate, in aqueous suspensions under mild conditions could result in the formation of three-dimensional (3-D) RGO hydrogel [38]. In this work, OA was used as a reducing agent. When heated, OA decomposed, liberating carbon dioxide gas. The gas embedded in the 3-D RGO hydrogel, and made the hydrogel full of porosity. The hydrogel can float on the water's surface because of the buoyancy of the gas bubbles embedded in it. The more pores embed in the hydrogel implied a lower density and a higher specific surface area of 3-D RGO aerogel made by freeze-dried method. Temperature is the key parameter for controlling the structure of the 3-D RGO hydrogel during the processing, since it plays an important role of reduction speed as well as adjusting working-temperature value. A series of experiments with two values of temperature has been investigated. The results show that 3-D RGO hydrogel has been obtained at the temperature 140 and 180 °C for 2 h. Figure 1 shows the top-view and side-view images of the 3-D RGO hydrogel cylinders.

Two 3-D RGO hydrogel cylinders shown in Fig. 1a, b were obtained at temperatures of 180 °C (left) and 140 °C (right), respectively. Although two cylinders were made using the same quantity of GO, the volume of the right cylinder is obviously larger than the left. This implies that there are more pores embed in the right cylinder; after freeze-drying; the aerogel made from the right would be more low-density. So the 3-D RGO hydrogel obtained at temperature of 140 °C was selected to be freeze-dried.

Characterization of 3-D RGO aerogel

After freeze drying, the 3-D RGO hydrogel cylinder became 3-D RGO aerogel cylinder. Figure 2 shows top-view (a) and side-view (b) photographs and cross-

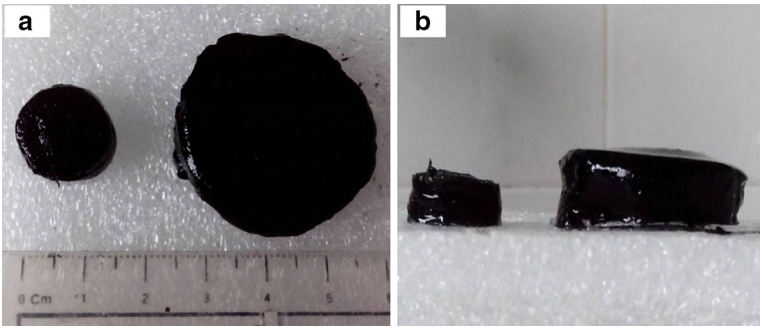

Fig. 1 Top-view (**a**) and side-view (**b**) images of 3-D RGO hydrogel cylinders obtained at temperatures of 180 °C (*left cylinder*), 140 °C (*right cylinder*) for 2 h

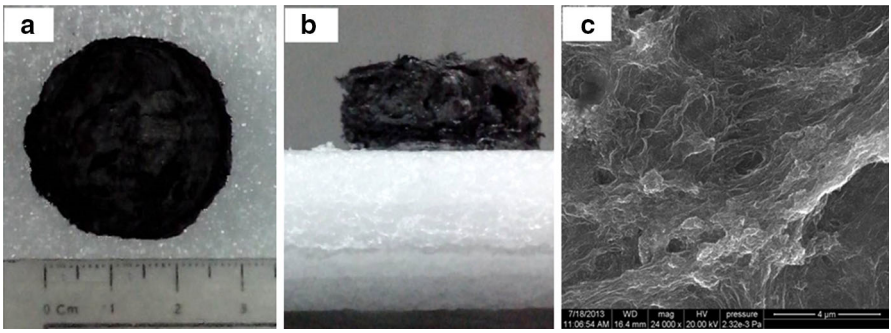

Fig. 2 Top-view (**a**) and side-view (**b**) photographs and cross-section SEM image (**c**) of the as-prepared 3-D RGO aerogel

section SEM image (c) of the aerogel, which was made from the 3-D RGO hydrogel reduced at 140 °C for 2 h. SEM image shows the aerogel is highly porous materials, in which the sizes of the pores are about 1–2 μm. Because of the porous feature, the aerogel cylinder is ultralight, and its apparent density was about 7.6 mg cm^{-3}.

The rheology properties of the as-prepared 3-D RGO aerogel cylinder were also studied. Figure 3 shows the axial compression tests' curve of the 3-D RGO aerogel cylinder. The curve shows an approximate linear region at longitudinal strain <70 %. The elastic modulus and yield stress of the 3-D RGO aerogel were measured to be about 0.00197 MPa and 1.38 kPa, respectively. When the longitudinal strain is >80 %, the 3-D RGO aerogel cylinder was yielded, and origin length cannot be recovered after stress withdrawing.

Figure 4 shows the X-ray diffraction (XRD) pattern of the as-prepared RGO aerogel after reduction at 140 °C for 2 h. If the background were deducted, all peeks would be very weak. The main diffraction peak at about 23° is very wide, indicating that the RGO aerogel is amorphous. The peaks appearing at 26° and 43° correspond to (002) and (100) diffractions of graphite, indicating the reformation of graphitic

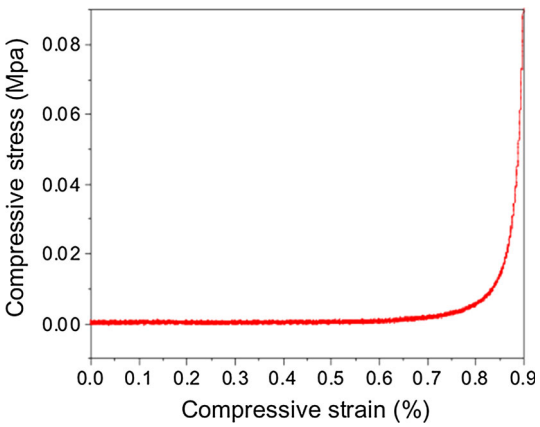

Fig. 3 Compressive stress–strain curve of 3-D RGO aerogel

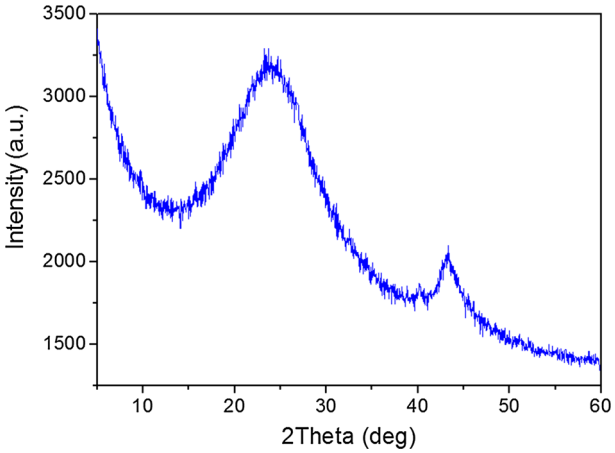

Fig. 4 XRD pattern of 3-D RGO aerogel

microcrystals on the graphene plane due to the chemical reduction of graphene oxide [38].

Figure 5 shows the FT-IR spectrum of GO and 3-D RGO aerogel. The band at 3400 cm^{-1} is attributed to the O–H stretching vibrations arising from hydroxyl groups in GO and RGO aerogel and water adsorbed on the 3-D RGO sheets; the absorption band at 1720 cm^{-1} is the characteristic band of C=O groups in carbonyl and carboxyl moieties; the band at 1220 cm^{-1} is assigned to the C–OH bonds [15]. In Fig. 5, all 3-D RGO aerogel adsorption bands mentioned above are weaker than GO, showing the GO has been reduced enough. On the other hand, the remaining hydroxyl groups on the 3-D RGO sheets can be the active centers for adsorption of pollutant ions in water according to the surface complexation model [39].

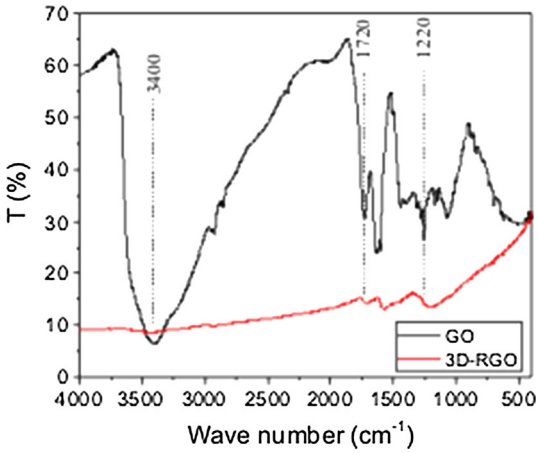

Fig. 5 FT-IR spectrum of GO and 3-D RGO aerogel

Adsorption properties

Kinetics of Hg^{2+} ions adsorption

The starting concentration of Hg^{2+} solution was 30.79 mg l^{-1}; the initial dosages of adsorbent (3-D RGO aerogel) were 20 mg in 100 ml solution. The adsorption kinetics of the adsorbent was determined by detecting the decrease in initial Hg^{2+} concentration. Figure 6a shows the kinetics of Hg^{2+} adsorption on the adsorbent in water.

The adsorption kinetics data were analyzed using pseudo-first-order and pseudo-second-order kinetic modes that were based on the assumptions that diffusion and chemisorption were the rate-determining steps, respectively [40]. The pseudo-first-order kinetic mode [41] can be described by Eq. (1):

$$Q = Q_e(1 - e^{-k_1 t}) \tag{1}$$

The pseudo-second-order kinetic mode [41] can be described by Eq. (2):

$$Q = \frac{k_2 Q_e^2 t}{1 + k_2 Q_e t} \tag{2}$$

where k_1, k_2 is the rate constant, and Q_e and Q are Hg^{2+} adsorption capacity at equilibrium and time (t), respectively. The experiment points are given in Fig. 6a. According to the two modes, after nonlinear least-square fitting of the experiment points, the fitting curves are also plotted in Fig. 6a and the fitting parameters Q_e, k_1, k_2, and R^2 (coefficient of determination) are displayed in Tables 1 and 2.

Kinetics of F^- adsorption

The starting concentration of F^- solution was 2.0 mg l^{-1}; the initial dosages of adsorbent (3D-RGO aerogel) were 15 mg in 100 ml solution. The adsorption kinetics of the 3-D RGO aerogel was determined by detecting the decrease in initial F^- concentration. Figure 6b shows the experiment points of F^- adsorption on the

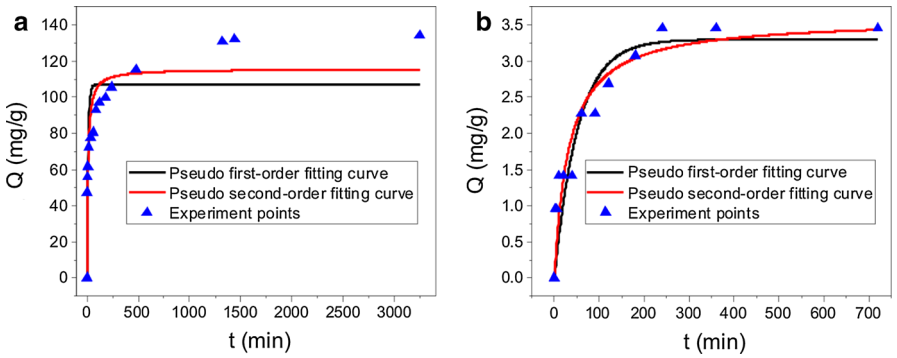

Fig. 6 Adsorption kinetics: **a** Hg^{2+} and **b** F^-. pH 6.0; 25 °C

Table 1 Rate constants and correlation coefficients of the pseudo-first-order kinetic modes

Adsorbate	Q_e (mg g^{-1})	k_1 (min^{-1})	R^2
Hg^{2+}	107	0.0853	0.668
F^-	3.30	0.0189	0.817

Table 2 Rate constants and correlation coefficients of the pseudo-second-order kinetic modes

Adsorbate	Q_e (mg g^{-1})	k_2 (g mg^{-1} min^{-1})	R^2
Hg^{2+}	116	0.000874	0.797
F^-	3.59	0.00858	0.866

3-D RGO aerogel in water. The fitting curves and parameters of adsorption kinetics are also obtained by the same computing methods as mentioned above (Fig. 6b).

Whether Hg^{2+} or F^- ions adsorption on the 3-D RGO aerogel in water, the pseudo-second-order kinetic mode's determination coefficient is obviously larger than the pseudo-first-order's (Tables 1, 2), which implies that adsorption follows the pseudo-second-order better than the pseudo-first-order kinetic mode.

According to Fig. 6 and Tables 1 and 2, it is apparent that the adsorption capacity of Hg^{2+} on the 3-D RGO aerogel was better than that of F^-.

Determination of adsorption isotherms

Langmuir and Freundlich adsorption isotherm models are used to determine the mechanistic parameters associated with Hg^{2+} and F^- adsorption [42, 43].

The Langmuir-type isotherm is indicative of chemisorption and a relatively high affinity between adsorbate and the adsorbent; the Langmuir isotherm model is suitable for single-layer adsorption onto a surface with a finite number of identical sites and uniform energies of adsorption with no transmigration of adsorbate in the plane of the surface [15]. The model is represented by Eq. (3):

$$\frac{1}{Q_e} = \frac{1}{Q_{max} K C_e} + \frac{1}{Q_{max}} \tag{3}$$

where C_e is the equilibrium concentration of the adsorbate (mg l^{-1}), Q_e is the equilibrium absorption capacity of adsorbate (mg g^{-1}), Q_{max} and K are Langmuir characteristic constants, indicating maximum adsorption capacity (mg g^{-1}) and the energy of adsorption (L mg^{-1}), respectively.

The Freundlich-type model is used when the adsorption process is assumed to take place on a heterogeneous surface that varies with surface coverage [3]. The Freundlich isotherm is represented by Eq. (4):

$$\ln Q_e = \ln k + (1/n) \ln C_e \tag{4}$$

where k and 1/n are the Freundlich characteristic constants, which indicate that the adsorption capacity and adsorption intensity. C_e and Q_e in Eq. (4) are the same as Eq. (3).

The isotherms of Hg^{2+} adsorption on RGO aerogel, which describe the relationship between the equilibrium absorption capacity of adsorbate (Q_e, mg g^{-1}) and the equilibrium concentration of adsorbate in the bulk solution (C_e, mg l^{-1}) at 25 °C, were studied here. The isotherm data of Hg^{2+} adsorption on the 3-D RGO aerogel in water are shown in Fig. 7. The experimental adsorption isotherms are shown in Fig. 7a. According to Eqs. (3) and (4), the plots of $1/Q_e$ versus $1/C_e$ and $\ln Q_e$ versus $\ln C_e$ are given in Fig. 7b, c. After linear regression in Fig. 7b, the obtained Langmuir-type adsorption isotherm parameters Q_{max}, K, and coefficient of determination (R^2) are displayed in Table 3. The Langmuir-type linear regression coefficient of determination ($R^2 = 0.992$), which is very close to 1, proving that Hg^{2+} adsorption on the 3-D RGO aerogel surface follows the Langmuir model very well. In order to compare with Langmuir-type models, Freundlich adsorption isotherm parameters k, n, and R^2 are also obtained by linear regression in Fig. 7c and listed in Table 3. The Freundlich linear regression coefficient of determination ($R^2 = 0.924$) is obviously less than the Langmuir-type ($R^2 = 0.992$), proving that Hg^{2+} adsorption on 3-D RGO aerogel surface follows the Langmuir model better by far than Freundlich.

The isotherm data of F^- adsorption on the 3-D RGO aerogel in water are shown in Fig. 8. The experimental adsorption isotherm is shown in Fig. 8a. The plots of $1/Q_e$ versus $1/C_e$ and $\ln Q_e$ versus $\ln C_e$ are given in Fig. 8b, c. The F^- adsorption constants and R^2 calculated using the two models are also listed in Table 3. According to the coefficient of determination (R^2), it is shown that the Langmuir model describes F^- adsorption on the 3-D RGO aerogel better than Freundlich model.

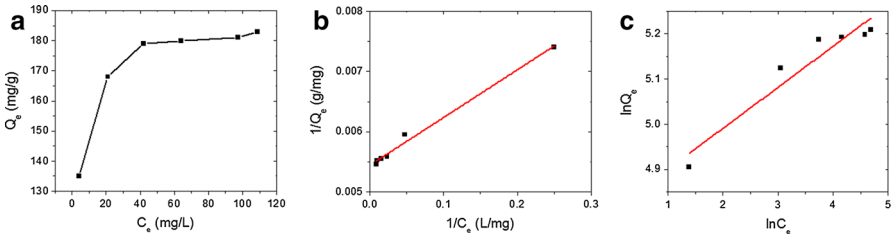

Fig. 7 Isotherms of Hg^{2+} adsorption on 3-D RGO aerogel: **a** Q_e versus C_e, **b** $1/Q_e$ versus $1/C_e$, and **c** $\ln Q_e$ versus $\ln C_e$. pH 6.0; 25 °C

Table 3 Coefficients of determination and isotherm constants for the Langmuir and Freundlich models

Isotherm type	Isotherm constants	Hg^{2+}	F^-
Langmuir	Q_{max} (mg g^{-1})	185	31.3
	K (L mg^{-1})	0.684	0.0786
	R^2	0.992	0.988
Freundlich	k (mg g^{-1}(mg L^{-1})$^{-1/n}$)	123	3.12
	n	11.0	1.92
	R^2	0.924	0.977

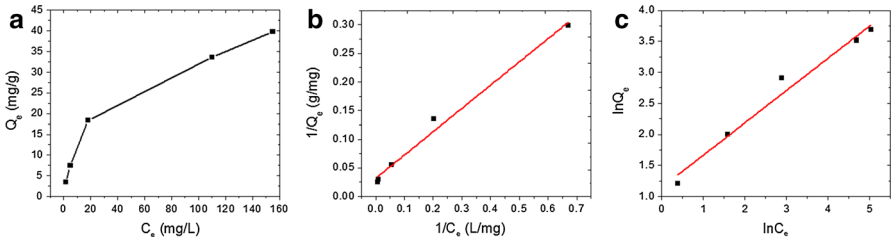

Fig. 8 Isotherms of F^- adsorption on 3-D RGO aerogel: **a** Q_e versus C_e, **b** $1/Q_e$ versus $1/C_e$ and **c** $\ln Q_e$ versus $\ln C_e$. pH 6.0; 25 °C

The max value Q_{max} of Hg^{2+} ions adsorption on the 3-D RGO aerogel is 185 mg g^{-1}. For comparison, the Q_{max} values of Hg^{2+} ions on other adsorbents are listed in Table 4. It can be seen that the 3-D RGO aerogel has much higher adsorption capacities than many other adsorbents. The high adsorption capacities suggest that 3-D RGO aerogel is a potential adsorbent for the removal of Hg^{2+} ions form wastewater.

The max value Q_{max} of F^- ions adsorption on the 3-D RGO aerogel is 31.3 mg g^{-1}. For comparison, the Q_{max} values of F^- ions on other adsorbents are listed in Table 5. It can also be seen that the 3-D RGO aerogel has much higher adsorption capacities than many other adsorbents. This indicates that 3-D RGO aerogel is a promising adsorbent for F^- ions' removal form water.

Adsorption thermodynamics

The thermodynamic parameters for Hg^{2+} ions adsorption on the 3-D RGO aerogel can be calculated from the temperature-dependent adsorption isotherms [60]. It is used to define whether the process is endothermic or exothermic and spontaneous. The effect of temperature on Hg^{2+} ions adsorption onto the 3-D RGO aerogel at pH 6.0 is given in Fig. 9a. Adsorption capacity is lowest at T = 318 K and highest at

Table 4 The comparison Hg^{2+} ions adsorption capacities for various adsorbents

Adsorbent	Experimental condition		Langmuir equation Q_{max} (mg g^{-1})	References
	pH	T (K)		
Filtrasorb 400	6	298	62.11	[44]
Rice husk ash	5.82	288	9.32	[45]
Chitosan spheres	6	298	13.5	[46]
Xanthi-Udic ferralosols	7	298	0.4167	[47]
$CoFe_2O_4$-rGO	4.6	298	157.9	[48]
Fe_3O_4	5	308	51.5	[49]
TiO_2	8	303	166.7	[50]
Magnetic CSTU	5	303	135	[51]
3-D RGO aerogel	6.0	298	185	This study

Table 5 The comparison F^- ions adsorption capacities for various adsorbents

Adsorbent	Experimental condition		Langmuir equation Q_{max} (mg g^{-1})	References
	pH	T (K)		
Protonated cross-linked chitosan particles	7.0	293	8.10	[52]
Granular ferric hydroxide	6.0–7.0	298	7.0	[53]
Manganese-oxide-coated alumina	7.0 ± 0.2	303 ± 2	2.851	[54]
Magnesia-loaded fly ash cenospheres	3.0	318	6.0	[55]
Alginate-oxalic acid-zirconium	Neutral	303	9.372	[56]
Hydroxyapatite	7.0	298	16.38	[57]
Charcoal	6.90 ± 0.10	298 ± 2	3.77	[58]
Chemically modified bentonite clay	7	303 ± 2	4.24	[59]
3-D RGO aerogel	6.0	298	31.3	This study

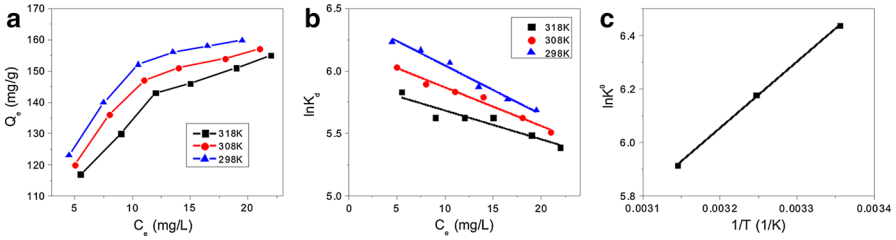

Fig. 9 The thermodynamics of Hg^{2+} adsorption on 3-D RGO aerogel: **a** Q_e versus C_e at 298, 308, and 318 K, **b** $\ln K_d$ versus C_e and **c** $\ln K^0$ versus 1/T. pH 6.0

T = 298 K, which shows that Hg^{2+} ions adsorption on the 3-D RGO aerogel is promoted at lower temperature. The standard free energy change (ΔG^0) can be calculated from the following Eq. (5):

$$\Delta G^0 = -RT \ln K^0 \tag{5}$$

where R is the universal gas constant (8.314 J mol^{-1} K^{-1}), T is the temperature in Kelvin. K^0 is the adsorption equilibrium constant. Values of $\ln K^0$ are obtained by plotting $\ln K_d$ (distribution coefficient) versus C_e (Fig. 9b) and extrapolating C_e to zero [61].

The standard enthalpy change (ΔH^0) and the standard entropy (ΔS^0) are then calculated from the linear plot of $\ln K^0$ versus 1/T for Hg^{2+} ions adsorption on the 3-D RGO aerogel in the following Eq. (6):

$$\ln K^0 = \frac{\Delta S^0}{R} - \frac{\Delta H^0}{RT} \tag{6}$$

Linear plot of $\ln K^0$ versus 1/T for the adsorption of Hg^{2+} ions on the 3-D RGO aerogel at 298, 318, and 338 K was give (Fig. 9c). Table 6 shows the obtained thermodynamic parameters of Hg^{2+} ion adsorption on the 3-D RGO aerogel. From

Table 6 Thermodynamic parameters of Hg^{2+} and F^- ion adsorption on the 3-D RGO aerogel

Ions	T (K)	ΔH^0 (kJ mol^{-1})	ΔS^0 (J mol^{-1})	ΔG^0 (kJ mol^{-1})
Hg^{2+}	298	−20.53	−15.37	−15.95
	308			−15.80
	318			−15.65
F^-	298	13.92	102.9	−16.51
	308			−17.48
	318			−18.45

Table 6 it can be found that the entropy change, ΔS^0, the enthalpy change, ΔH^0, and the standard free energy change, ΔG^0 at 298, 318, and 338 K, respectively. The negative ΔH^0 value suggests that Hg^{2+} ion adsorption on the surface of the 3-D RGO aerogel is an exothermal process, which is favorable for Hg^{2+} ions adsorption on the 3-D RGO aerogel. Negative ΔG^0 value indicates that the adsorption of Hg^{2+} ions on the 3-D RGO aerogel is a spontaneous process.

The effect of temperature on F^- ions adsorption onto the 3-D RGO aerogel at pH 6.0 is given in Fig. 10a. The thermodynamic parameters of F^- ion adsorption onto the 3-D RGO aerogel at pH 6.0 was obtained using a similar method mentioned above (Fig. 10b, c). Table 6 also shows the obtained thermodynamic parameters of F^- ions adsorption on the 3-D RGO aerogel in water. The positive ΔH^0 value shows that F^- ion adsorption on the surface of the 3-D RGO aerogel is an endothermic process. A negative ΔG^0 value indicates that the adsorption of F^- ions on the 3-D RGO aerogel is also a spontaneous process.

Regeneration properties

In order to evaluate the reversibility of Hg^{2+} and F^- ion adsorption on the 3-D RGO aerogel, regeneration properties were also determined. The relationship between Hg^{2+} and F^- ion removal rate and the rounds of the 3-D RGO aerogel's use is shown in Fig. 11.

According to Fig. 11, the Hg^{2+} and F^- ion removal rates of the first-round adsorption were best, where the removal rates were 66 and 45 %, respectively. When the round increased, removal rates decreased slightly. At the 5th round, Hg^{2+}

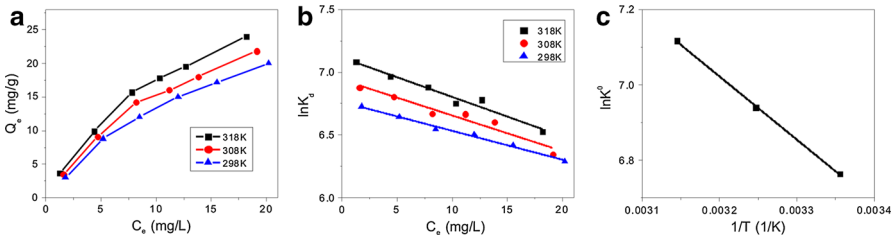

Fig. 10 Thermodynamics of F^- adsorption on 3-D RGO aerogel: **a** Q_e versus C_e at 298, 308, 318 K, **b** $\ln K_d$ versus C_e, and **c** $\ln K^0$ versus 1/T. pH 6.0

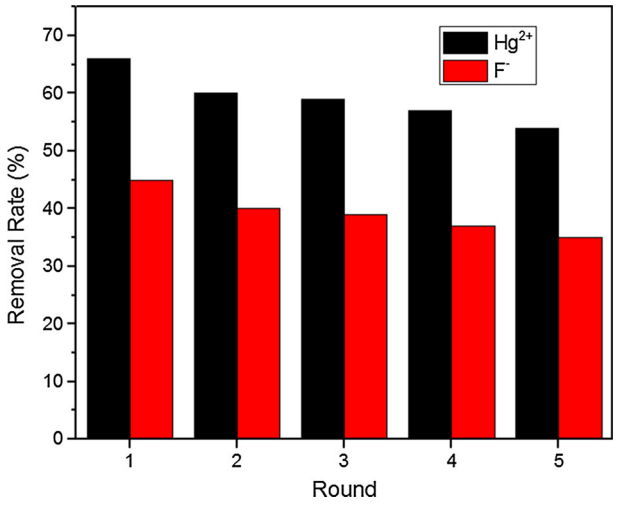

Fig. 11 Relationship between Hg^{2+} and F^- ion removal rate versus the use round of adsorbent

and F^- ion removal rates remained 54 and 35 %, respectively. Figure 11 shows promising regeneration properties of Hg^{2+} and F^- ions adsorption on the 3-D RGO aerogel in water.

Adsorption mechanism

The FT–IR spectra of 3-D RGO aerogel is shown in Fig. 5. The peaks at 1220 and 3400 cm^{-1} indicate that there are plenty of hydroxyl groups linked with carbon atoms on graphene plain in the aerogel. The groups could be the center of Hg^{2+} ion adsorption [39]. The adsorption of Hg^{2+} ions on 3-D RGO aerogel is governed by the cation exchange reaction of Hg^{2+} ions on the RGO surface [60]. The reaction can be described as shown in Fig. 12.

According to Le. Chatelier's principle, at low pH, 3-D RGO aerogel binds to Hg^{2+} ions more difficultly than at high pH. This hypothesis was supported by the

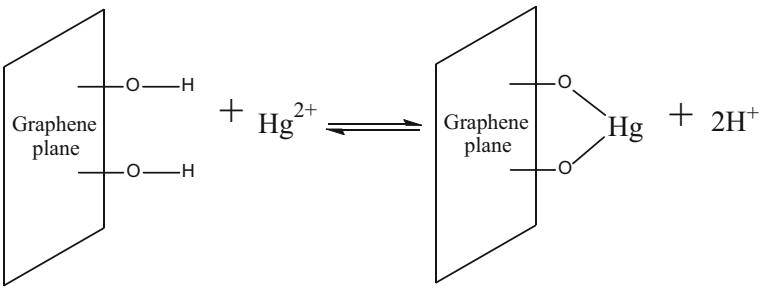

Fig. 12 Diagram of Hg^{2+} ion adsorption on 3-D RGO aerogel sorbent

fact that aerogel saturated by Hg^{2+} ions could be regenerated by strong acid aqueous solution.

Delocalized π electrons (–Cπ) are known to be largely responsible for the basicity of the carbon atoms on the graphene plane in 3-D RGO aerogel because the following equilibrium (formula (7)) is established in aqueous solution [44].

$$-C\pi + 2H_2O \rightleftharpoons -C\pi-H_3O^+ + OH^- \quad (7)$$

Thus, it can be proposed that $-C\pi-H_3O^+$ could attract F^- ions via electrostatic force for F^- adsorption to take place. The reaction can be described in formula (8).

$$-C\pi-H_3O^+ + F^- \rightleftharpoons -C\pi-H_3OF \quad (8)$$

This mechanism was also supported by the fact that aerogel saturated could be regenerated by strong base aqueous solution according to Le. Chatelier's principle.

Conclusions

Three-dimensional (3-D) reduced-graphene oxide (RGO) hydrogel was synthesized in a Teflon-lined autoclave by the reduction of graphene oxide using oxalic acid dihydrate. The porous and low-density 3-D RGO aerogel was prepared after the as-prepared RGO hydrogel was freeze-dried to remove absorbed water. The application of the 3-D RGO aerogel as an adsorbent for the removal of the inorganic ions, Hg^{2+} and F^-, from aqueous solutions was investigated. The 3-D RGO aerogel showed excellent removal capabilities and speed for Hg^{2+} and F^-. Hg^{2+} and F^- captured by the 3-D RGO aerogel follow the pseudo-second-order kinetic mode very well. Hg^{2+} and F^- adsorption on the 3-D RGO aerogel surface follows the Langmuir model better than the Freundlich model. The maximum adsorption capability for Hg^{2+} and F^- approached 185 and 31.3 mg g^{-1}, respectively, indicating that the 3-D RGO aerogel is a very suitable material for environmental pollution management.

Acknowledgments The authors gratefully acknowledge financial support from the Postgraduate Academic Innovation and Research Project Foundation of Anhui University (yqh100056), the National Natural Science Foundation of China (21177131 and 21277146), and Key Technologies R & D Program of Anhui Province (1501021005).

References

1. Y. Wang, Y. Qi, Y. Li, J. Wu, X. Ma, C. Yu, L. Ji, Preparation and characterization of a novel nano-absorbent based on multi-cyanoguanidine modified magnetic chitosan and its highly effective recovery for Hg(II) in aqueous phase. J. Hazard. Mater. **260**, 9–15 (2013)
2. V.B.H. Dang, H.D. Doan, T. Dang-Vu, A. Lohi, Equilibrium and kinetics of biosorption of cadmium(II) and copper(II) ions by wheat straw. Bioresour. Technol. **100**, 211–219 (2009)
3. M. Baunthiyal, S. Ranghar, Accumulation of fluoride by plants: potential for phytoremediation. CLEAN Soil Air Water **43**, 127–132 (2015)

4. X.H. Guan, J.S. Du, X.G. Meng, Y.K. Sun, B. Sun, Q.H. Hu, Application of titanium dioxide in arsenic removal from water: a review (vol 215, pg 1, 2012). J. Hazard. Mater. **221**(2012), 303 (2012)
5. D. Ballestero, C. Gomez-Gimenez, E. Garcia-Diez, R. Juan, B. Rubio, M.T. Izquierdo, Influence of temperature and regeneration cycles on Hg capture and efficiency by structured Au/C regenerable sorbents. J. Hazard. Mater. **260**, 247–254 (2013)
6. H.Y. Jin, Z.J. Ji, J. Yuan, J. Li, M. Liu, C.H. Xu, J. Dong, P. Hou, S. Hou, Research on removal of fluoride in aqueous solution by alumina-modified expanded graphite composite. J. Alloys Compd. **620**, 361–367 (2015)
7. S. Vasudevan, B.S. Kannan, J. Lakshmi, S. Mohanraj, G. Sozhan, Effects of alternating and direct current in electrocoagulation process on the removal of fluoride from water. J. Chem. Technol. Biotechnol. **86**, 428–436 (2011)
8. S. Vasudevan, J. Lakshmi, G. Sozhan, Optimization of electrocoagulation process for the simultaneous removal of mercury, lead, and nickel from contaminated water. Environ. Sci. Pollut. Res. **19**, 2734–2744 (2012)
9. S. Vasudevan, J. Lakshmi, G. Sozhan, Studies on the removal of arsenate by electrochemical coagulation using aluminum alloy anode. CLEAN Soil Air Water **38**, 506–515 (2010)
10. C. Amor, E. De Torres-Socias, J.A. Peres, M.I. Maldonado, I. Oller, S. Malato, M.S. Lucas, Mature landfill leachate treatment by coagulation/flocculation combined with Fenton and solar photo-Fenton processes. J. Hazard. Mater. **286**, 261–268 (2015)
11. K. Gopal, S.B. Srivastava, S. Shukla, J.L. Bersillon, Contaminants in drinking water and its mitigation using suitable adsorbents: an overview. J. Environ. Biol. **25**, 469–475 (2004)
12. I.H. Lee, Y.C. Kuan, J.M. Chern, Equilibrium and kinetics of heavy metal ion exchange. J. Chin. Inst. Chem. Eng. **38**, 71–84 (2007)
13. X.F. Zhai, J.Q. Meng, R. Li, L. Ni, Y.F. Zhang, Hypochlorite treatment on thin film composite RO membrane to improve boron removal performance. Desalination **274**, 136–143 (2011)
14. L.J. Banasiak, B. Van der Bruggen, A.I. Schafer, Sorption of pesticide endosulfan by electrodialysis membranes. Chem. Eng. J. **166**, 233–239 (2011)
15. J.N. Tiwari, K. Mahesh, N.H. Le, K.C. Kemp, R. Timilsina, R.N. Tiwari, K.S. Kim, Reduced graphene oxide-based hydrogels for the efficient capture of dye pollutants from aqueous solutions. Carbon **56**, 173–182 (2013)
16. V. Chandra, J. Park, Y. Chun, J.W. Lee, I.C. Hwang, K.S. Kim, Water-dispersible magnetite-reduced graphene oxide composites for arsenic removal. ACS Nano **4**, 3979–3986 (2010)
17. Y. He, Y. Liu, T. Wu, J. Ma, X. Wang, Q. Gong, W. Kong, F. Xing, J. Gao, An environmentally friendly method for the fabrication of reduced graphene oxide foam with a super oil absorption capacity. J. Hazard. Mater. **260**, 796–805 (2013)
18. S. Bae, H. Kim, Y. Lee, X.F. Xu, J.S. Park, Y. Zheng, J. Balakrishnan, T. Lei, H.R. Kim, Y.I. Song, Y.J. Kim, K.S. Kim, B. Ozyilmaz, J.H. Ahn, B.H. Hong, S. Iijima, Roll-to-roll production of 30-inch graphene films for transparent electrodes. Nat. Nanotechnol. **5**, 574–578 (2010)
19. K.S. Kim, Y. Zhao, H. Jang, S.Y. Lee, J.M. Kim, K.S. Kim, J.H. Ahn, P. Kim, J.Y. Choi, B.H. Hong, Large-scale pattern growth of graphene films for stretchable transparent electrodes. Nature **457**, 706–710 (2009)
20. M.J. Allen, V.C. Tung, R.B. Kaner, Honeycomb carbon: a review of graphene. Chem. Rev. **110**, 132–145 (2010)
21. A.K. Geim, Graphene: status and prospects. Science **324**, 1530–1534 (2009)
22. S.K. Min, W.Y. Kim, Y. Cho, K.S. Kim, Fast DNA sequencing with a graphene-based nanochannel device. Nat. Nanotechnol. **6**, 162–165 (2011)
23. W.Y. Kim, K.S. Kim, Prediction of very large values of magnetoresistance in a graphene nanoribbon device. Nat. Nanotechnol. **3**, 408–412 (2008)
24. J.H. Seol, I. Jo, A.L. Moore, L. Lindsay, Z.H. Aitken, M.T. Pettes, X.S. Li, Z. Yao, R. Huang, D. Broido, N. Mingo, R.S. Ruoff, L. Shi, Two-dimensional phonon transport in supported graphene. Science **328**, 213–216 (2010)
25. S.Y. Park, J. Park, S.H. Sim, M.G. Sung, K.S. Kim, B.H. Hong, S. Hong, Enhanced differentiation of human neural stem cells into neurons on graphene. Adv. Mater. **23**, H263 (2011)
26. J.N. Tiwari, R.N. Tiwari, K.S. Kim, Zero-dimensional, one-dimensional, two-dimensional and three-dimensional nanostructured materials for advanced electrochemical energy devices. Prog. Mater. Sci. **57**, 724–803 (2012)

27. J.N. Tiwari, R.N. Tiwari, G. Singh, K.L. Lin, Direct synthesis of vertically interconnected 3-D graphitic nanosheets on hemispherical carbon particles by microwave plasma CVD. Plasmonics **6**, 67–73 (2011)
28. J.N. Tiwari, R.N. Tiwari, Y.M. Chang, K.L. Lin, A promising approach to the synthesis of 3D nanoporous graphitic carbon as a unique electrocatalyst support for methanol oxidation. Chemsuschem **3**, 460–466 (2010)
29. R.N. Tiwari, M. Ishihara, J.N. Tiwari, M. Yoshimura, Transformation of polymer to graphene films at partially low temperature. Polym. Chem. **3**, 2712–2715 (2012)
30. R.N. Tiwari, M. Ishihara, J.N. Tiwari, M. Yoshimura, Flame-annealing-assisted synthesis of graphene films from adamantane (vol 22, pg 15031, 2012). J. Mater. Chem. **22**(2012), 25496 (2012)
31. S. Chowdhury, R. Balasubramanian, Recent advances in the use of graphene-family nanoadsorbents for removal of toxic pollutants from wastewater. Adv. Colloid Interface **204**, 35–56 (2014)
32. P. Ganesan, R. Kamaraj, S. Vasudevan, Application of isotherm, kinetic and thermodynamic models for the adsorption of nitrate ions on graphene from aqueous solution. J. Taiwan Inst. Chem. Eng. **44**, 808–814 (2013)
33. J. Lakshmi, S. Vasudevan, Graphene—a promising material for removal of perchlorate (ClO_4 (−)) from water. Environ. Sci. Pollut. Rev. **20**, 5114–5124 (2013)
34. S. Vasudevan, J. Lakshmi, The adsorption of phosphate by graphene from aqueous solution. RSC Adv. **2**, 5234–5242 (2012)
35. W. Chen, L. Yan, In situ self-assembly of mild chemical reduction graphene for three-dimensional architectures. Nanoscale **3**, 3132–3137 (2011)
36. Z. Fan, D.Z.Y. Tng, S.T. Nguyen, J.D. Feng, C.F. Lin, P.F. Xiao, L. Lu, H.M. Duong, Morphology effects on electrical and thermal properties of binderless graphene aerogels. Chem. Phys. Lett. **561**, 92–96 (2013)
37. W.S. Hummers, R.E. Offeman, Preparation of graphitic oxide. J. Am. Chem. Soc. **80**, 1339 (1958)
38. W.F. Chen, L.F. Yan, In situ self-assembly of mild chemical reduction graphene for three-dimensional architectures. Nanoscale **3**, 3132–3137 (2011)
39. L. Sigg, W. Stumm, The interaction of anions and weak acids with the hydrous goethite (alpha-FeOOH) surface. Colloid Surf. **2**, 101–117 (1981)
40. W.S.W. Ngah, N.F.M. Ariff, A. Hashim, M.A.K.M. Hanafiah, Malachite Green adsorption onto chitosan-coated bentonite beads: isotherms, kinetics and mechanism. CLEAN Soil Air Water **38**, 394–400 (2010)
41. S. Karmaker, T. Sen, T.K. Saha, Adsorption of reactive yellow 145 onto chitosan in aqueous solution: kinetic modeling and thermodynamic analysis. Polym. Bull. **72**, 1879–1897 (2015)
42. I. Langmuir, The constitution and fundamental properties of solids and liquids part I solids. J. Am. Chem. Soc. **38**, 2221–2295 (1916)
43. H. Freundlich, Concerning adsorption in solutions. Z. Phys. Chem-Stoch Ve **57**, 385–470 (1906)
44. M.S. Polo, J.R. Utrilla, Adsorbent-adsorbate interactions in the adsorption of Cd(II) and Hg(II) on ozonized activated carbons. Environ. Sci. Technol. **36**, 3850–3854 (2002)
45. Q.G. Feng, Q.Y. Lin, F.Z. Gong, S. Sugita, M. Shoya, Adsorption of lead and mercury by rice husk ash. J. Colloid Interface Sci. **278**, 1–8 (2004)
46. R.S. Vieira, M.M. Beppu, Dynamic and static adsorption and desorption of Hg(II) ions on chitosan membranes and spheres. Water Res. **40**, 1726–1734 (2006)
47. Y.K. Yang, L. Liang, D.Y. Wang, Effect of dissolved organic matter on adsorption and desorption of mercury by soils. J. Environ. Sci. China **20**, 1097–1102 (2008)
48. Y.K. Zhang, L.G. Yan, W.Y. Xu, X.Y. Guo, L.M. Cui, L. Gao, Q. Wei, B. Du, Adsorption of Pb(II) and Hg(II) from aqueous solution using magnetic $CoFe_2O_4$-reduced graphene oxide. J. Mol. Liq. **191**, 177–182 (2014)
49. S.D. Pan, Y. Zhang, H.Y. Shen, M.Q. Hu, An intensive study on the magnetic effect of mercapto-functionalized nano-magnetic Fe_3O_4 polymers and their adsorption mechanism for the removal of Hg(II) from aqueous solution. Chem. Eng. J. **210**, 564–574 (2012)
50. Z. Ghasemi, A. Seif, T.S. Ahmadi, B. Zargar, F. Rashidi, G.M. Rouzbahani, Thermodynamic and kinetic studies for the adsorption of Hg(II) by nano-TiO_2 from aqueous solution. Adv. Powder Technol. **23**, 148–156 (2012)
51. M. Monier, D.A. Abdel-Latif, Preparation of cross-linked magnetic chitosan-phenylthiourea resin for adsorption of Hg(II), Cd(II) and Zn(II) ions from aqueous solutions. J. Hazard. Mater. **209**, 240–249 (2012)

52. R.H. Huang, B.C. Yang, Q. Liu, K.L. Ding, Removal of fluoride ions from aqueous solutions using protonated cross-linked chitosan particles. J. Fluor. Chem. **141**, 29–34 (2012)
53. E. Kumar, A. Bhatnagar, M. Ji, W. Jung, S.H. Lee, S.J. Kim, G. Lee, H. Song, J.Y. Choi, J.S. Yang, B.H. Jeon, Defluoridation from aqueous solutions by granular ferric hydroxide (GFH). Water Res. **43**, 490–498 (2009)
54. S.M. Maliyekkal, A.K. Sharma, L. Philip, Manganese-oxide-coated alumina: a promising sorbent for defluoridation of water. Water Res. **40**, 3497–3506 (2006)
55. X.T. Xu, Q. Li, H. Cui, J.F. Pang, L. Sun, H. An, J.P. Zhai, Adsorption of fluoride from aqueous solution on magnesia-loaded fly ash cenospheres. Desalination **272**, 233–239 (2011)
56. S.M. Prabhu, S. Meenakshi, Novel one-pot synthesis of dicarboxylic acids mediated alginate-zirconium biopolymeric complex for defluoridation of water. Carbohydr. Polym. **120**, 60–68 (2015)
57. Y.L. Nie, C. Hu, C.P. Kong, Enhanced fluoride adsorption using Al(III) modified calcium hydroxyapatite. J. Hazard. Mater. **233**, 194–199 (2012)
58. E. Tchomgui-Kamga, E. Ngameni, A. Darchen, Evaluation of removal efficiency of fluoride from aqueous solution using new charcoals that contain calcium compounds. J. Colloid Interface Sci. **346**, 494–499 (2010)
59. S.P. Kamble, P. Dixit, S.S. Rayalu, N.K. Labhsetwar, Defluoridation of drinking water using chemically modified bentonite clay. Desalination **249**, 687–693 (2009)
60. S.B. Wu, K.S. Zhang, X.L. Wang, Y. Jia, B. Sun, T. Luo, F.L. Meng, Z. Jin, D.Y. Lin, W. Shen, L.T. Kong, J.H. Liu, Enhanced adsorption of cadmium ions by 3D sulfonated reduced graphene oxide. Chem. Eng. J. **262**, 1292–1302 (2015)
61. Y. Li, P. Zhang, Q. Du, X. Peng, T. Liu, Z. Wang, Y. Xia, W. Zhang, K. Wang, H. Zhu, D. Wu, Adsorption of fluoride from aqueous solution by graphene. J. Colloid Interface Sci. **363**, 348–354 (2011)